Analytica Chimica Acta 1107 (2020) 92–100

Contents lists available at ScienceDirect

Analytica Chimica Acta

journal homepage: www.elsevier.com/locate/aca

High throughput lipid profiling for subtype classification of hepatocellular carcinoma cell lines and tumor tissues

Tao Wang [a], Xiaoming Chen [a], Chunyan Luan [b], Jianmin Wu [a, *]

[a] Institution of Analytical Chemistry, Department of Chemistry, Zhejiang University, Hangzhou, 310058, China
[b] Well-Healthcare Technologies, Co. LTD, Hangzhou, 310051, China

HIGHLIGHTS

- A nanostructure assisted LDI chip was developed for high throughput detection of cell lipids.
- A good repeatability of cell lipid profile could be obtained by inner-cluster data normalization method.
- Five types of hepatocellular carcinoma cell lines were successfully differentiated by the established statistical model.
- The cell recognition model could identify cell subtype in mixed cells, xenogeneic tumor tissues, and drug-treated cells.

GRAPHICAL ABSTRACT

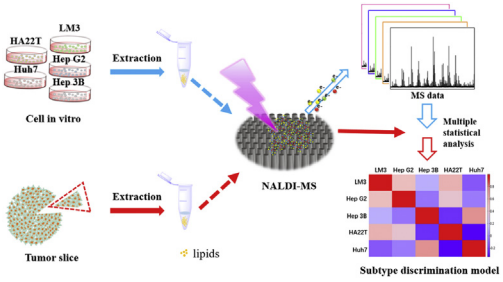

ARTICLE INFO

Article history:
Received 1 January 2020
Received in revised form
4 February 2020
Accepted 9 February 2020
Available online 12 February 2020

Keywords:
Matrix-free laser desorption/ionization
High throughput silicon nanowires array chip
Lipidomics
Cell and tissue subtype
Drug susceptibility

ABSTRACT

Cell heterogeneity of tumor tissues is one of the causes of cancer recurrence after chemotherapy. Cell subtype identification in tumor tissues of specific cancer is critical for precision medicine and prognosis. As the structural and functional components of cells, lipids are closely related to the apparent morphology of cells. They are potential biomarkers of species of cancers and can be used to classify different cancer cell types, but it remains a challenge to establish a stable cell differentiation model and extend it to tumor tissue cell subtype differentiation. Here we describe a lipid profiling method based on nanostructure assisted laser desorption/ionization mass spectrometry (NALDI-MS), which could classify five hepatocellular carcinoma (HCC) cell lines and discriminate subtype of mixed cells and tumor tissues. The NALDI target was patterned with array of sample spots containing vertical silicon nanowires (Si NWs). Owing to its high ability to absorb laser energy, the vertical Si NWs can help to generate abundant lipid ions of cell extracts without need of organic matrix. Combined with statistical analysis methods, twenty-two ion peaks distributed in four MS peak clusters were selected as potential biomarkers to distinguish the subtype of the five HCC cell lines. Peak normalization was performed within each MS peak cluster to reduce the variation of peak intensity in batch to batch analysis. Compared to full-spectrum normalization method, the inner-cluster normalization method could help to distinguish cell subtype more stably and accurately. The molecular structure of these biomarkers was identified and sorted into two classes including phosphatidylcholine (PE, PI, PG, PA, PS) and glycosphingolipid (LacCer, ST). Furthermore, the established method was successfully applied to identify the major HCC cell subtype

* Corresponding author.
E-mail address: wjm-st1@zju.edu.cn (J. Wu).

https://doi.org/10.1016/j.aca.2020.02.019

in mixed cell samples and xenograft tumor tissues as well as drug response test, showing great potential in precision medicine and prognosis.

Abbreviations

PE	phosphatidylethanolamine
PI	phosphatidylinositol
PG	phosphatidyl glycerol
PA	phosphatidic acid
PS	phosphatidylserine
LacCer	lactosyl ceramide
ST	sulfatide
FA	fatty acid

1. Introduction

Hepatocellular carcinoma (HCC) is the most common malignancy in liver cancer with poor prognosis that leading to cancer-related death [1]. With the advance in precise medical solutions for cancer treatment in recent years [2], personalized medicine for HCC patients will be achieved. However, tumor heterogeneity might be a challenge for realizing precision medicine [3]. Tumor heterogeneity is influenced by the genetic and epigenetic differences among cancer cells themselves [4,5], and is related to the poor prognosis, resistance to medicine and the high metastasis capability in clinical cancer treatments [6,7]. Thus the discrimination of cancer cell subtype in tumors is critical to reveal the tumor heterogeneity and provide the basis of precise medical solutions for clinical cancer patients.

Currently, gene expression profiling (GEP) [8–10] and immunohistochemistry (IHC) [11–13] are the common methods to classify cancer subtype, which focus on genomics and proteomics. As the downstream of genomics and proteomics, metabolomics depicts real-time biochemical activity of cells and therefore plays an important role in phenotype research at cells and even tissue levels. Lipids are the structural components of cell membranes [14]. The synthesis and degradation of lipids play the vital role in energy storage, production and cell signalling [14]. Recently, studies on lipidomics have made a great contribution to the discovery of novel lipid biomarkers in specific cancers [15–19].

Mass spectrometry (MS) has become one of the most powerful tools in lipidomics research [20] with its high sensitivity, multiple detection and molecular identification abilities. Apart from the traditional LC/GC-MS, the development of high-throughput mass spectrometry without LC step is urgently needed in rapid clinical diagnosis. Matrix assisted laser desorption/ionization (MALDI) MS is considered as a promising platform with high throughput for proteomics and lipidomics research. MALDI-MS has been applied in biotyping [21] of mammalian cells [22–25], intrinsic subtyping of tumor tissues [26,27] and tissue imaging [28,29]. However, detection of small molecules with molecular weights below 700 Da using MALDI-MS could be interfered by the signal derived from adduct ions of traditional organic matrix [30]. To overcome this problem, various nanostructured carbon materials [31,32], metal materials [33–35] and silicon materials [36–39] have been employed as LDI substrates to desorb and ionize analytes under laser irradiation. Desorption–ionization on porous silicon (DIOS) [36], nanostructure initiator mass spectrometry (NIMS) [40], nanostructure assisted LDI (NALDI) [41] and surface assisted LDI (SALDI) [42] have been developed as complementary of MALDI. Among them, NALDI has been used for the analysis of various lipids [43,44] and MS imaging of organic tissues [45] and tumor tissues [46] with high sensitivity. Silicon nanowire (bandgap of silicon = 1.12 eV) has emerged to be a good candidate as NALDI substrate owing to its large surface area, high laser energy absorption and efficient energy-transfer ability [47–49]. However, high throughput MS detection of cell samples using array-based chip is still need to be developed, since a formulated array-based chip can facilitate high throughput profiling of lipids extracted from cells. That will lead to the finding of stable and reliable biomarkers associated with the cell subtype of tumor tissues.

Herein, we developed a NALDI target containing vertical Si NWs array to detect lipids extracted from five HCC cell lines. The patterned spots on NALDI target can effectively limit the diffusion of sample solution and improve the repeatability and accuracy in MS detection of lipid samples. To further reduce the data variation in the acquisition of lipid profile, an inner-cluster normalization method was proposed. Compared with the method of data normalization within entire MS spectrum, the inner-cluster normalization resulted in better repeatability and stability. After statistical analysis, twenty-two peaks from four ion clusters were discovered and used as potential biomarkers that could discriminate five subtypes of HCC cell lines successfully. Lipid profiles of mice xenogeneic tumors were detected and analyzed statistically, and the results proved that the differentiation model based on the panel of lipid biomarkers can also identify cell subtype in tissue samples with high accuracy. Furthermore, we also demonstrated that the cell lipid profile was very sensitive to anticancer drug treatment.

2. Materials and methods

2.1. Chemicals and materials

Silicon wafers (n-type, 1–10 Ω cm, <100>) were purchased from Lijing Silicon Materials Co. (Quzhou, China). Photoresist (AZ4620) was purchased from AZ Electronic Materials (Japan). Hydrofluoric acid (HF, 40%) was obtained from Sinopharm Chemical Reagent Co. (Shanghai, China). Silver nitrate ($AgNO_3$), acetone, 3-(4,5-dimethylthiazol-2-yl)-2,5-diphenyltetrazolium bromide (MTT), dimethyl sulfoxide (DMSO), dichloromethane (CH_2Cl_2) HPLC degree and methanol HPLC degree were purchased from Aladdin Co. (Shanghai, China). Alpha-cyano-4-hydroxycinnamic acid (α-CHCA) and 2, 5-dihydroxybenzoic acid (DHB) were purchased form Bruker Daltonics Inc. (Billerica, USA). Lauric acid (C12:0), palmitic acid (C16:0), stearic acid (C18:0), arachidic acid (C20:0), teracosanoic acid (C24:0), 1,2-dipalmitoyl-sn-glycero-3-phosphoethanolamine (DPPE 16:0/16:0) were purchased from Aladdin Co. (Shanghai, China). Sorafenib was purchased from Santa Cruz Biotechnology (Dallas, U.S.A.). The Dulbecco's modified eagle medium (DMEM) was purchased from Sigma-Aldrich (Saint Louis, MO, U.S.A.). The trypsin-EDTA and antibiotics were purchased from Gibco Corp. (Grand Island, NY, USA). Fetal bovine serum (FBS) was purchased from Biological Industries Corp. (Israel). Five HCC cell lines were

used, HCCLM3 (LM3), HA22T and Huh7 cells were obtained from the Cell Bank of the Chinese Academy of Science (Shanghai, China). Hep G2 and Hep 3B were obtained from the American Tissue Culture Collection (ATCC). The male nude mice were purchased from Slack Corp. (Shanghai, China). All other reagents used in this experiment were of analytical reagent grade.

2.2. Preparation of NALDI target

The silicon NALDI target was fabricated by photolithography procedure and the one-step metal assisted chemical etching (MACE) method. A 4-inch silicon wafer was cut into pieces with size of 4 cm × 3 cm. After cleaning with acetone and ethanol, the silicon wafers were spin-coated with an AZ4620 photoresist and pre-baked at 95 °C for 3 min. Then the wafer covered with a designed photomask (8 × 6 holes array, the hole diameter is 3 mm) was exposed to UV light and then developed in 0.07% NaOH aqueous solution for 3 min. After a post-bake procedure at 115 °C for 10 min, the silicon wafer was washed by DI water and dried under a dry nitrogen stream. The exposed area of patterned silicon wafer was immersed into an etching solution containing 4.8 M HF and 0.02 M $AgNO_3$ for 10 min (caution: HF is highly toxic and contact with skin should be avoided). After etching, the wafer was washed by DI water for three times and then immersed into diluted HNO_3 (v/v = 1:1) for 30 min to dissolve the silver on the nanowire surface. Acetone was used to remove the residual photoresist. The prepared NALDI target with an array of identical Si NWs spots was washed by the DI water and then dried by nitrogen stream. Non-array targets were prepared in the same way as above, but without the photolithography process. Then the etched wafer was cut into pieces with a size of 3 mm × 3 mm.

2.3. Cell culture

Five types of HCC cell lines were used in this study, including LM3, Hep G2, Hep 3B, HA22T and Huh7. All cell lines were cultured in DMEM with 10% FBS and incubated in an incubator filled with 5% CO_2 and 95% air at 37 °C. When the cells were grown to 85% confluence, they were treated with 0.25% trypsin–EDTA, and then washed by PBS for three times. Each type of cell lines was re-suspended in PBS at the concentration of 1×10^7 cells mL^{-1}. For each cell line, three replicated samples were collected and stored in the − 80 °C refrigerator before use.

2.4. Tissue preparation

After cell culture, the LM3 cells and the Huh7 cells were centrifuged and re-suspended in DMEM with 5% FBS at the concentration of 1×10^7 cells mL^{-1}. The two types of cell lines were mixed homogeneously at the following ratio: 100% LM3, 75% LM3+25% Huh7, 25% LM3+75% Huh7, 100% Huh7. Then, each type of mixed cell sample containing 1×10^6 cells was subcutaneously injected to a male mouse, respectively. After the size of xenografted tumors reached to ~1 cm, the tumor tissues were collected and stored at −80 °C before use. All animal experimental protocols were approved by the Laboratory Animal Center of Zhejiang Academy of Medical Sciences.

2.5. Preparation of sorafenib treated cells

LM3 cell line was chosen for anticancer drug susceptibility test. Briefly, LM3 cells were seeded into 6-well plates (3×10^5 cells per well) and cultured overnight before sorafenib treated. For sorafenib treatment, cells in the wells were treated with DMEM containing different concentrations of sorafenib (0 [control], 0.312 μM, 5 μM) and incubated for 24 h. Then the cells were trypsinized and washed by PBS for three times before collection. The MTT assay was performed to assess the influence of sorafenib on LM3 cells. LM3 cells were seeded onto 96-well plates (1×10^4 cells per well) and cultured overnight, then cultured with DMEM containing different concentrations of sorafenib (0 μM, 0.312 μM, 5 μM) for 24 h. Each drug concentration has 5 replicated wells. After 24 h, 10 μL of MTT reagent (5 mg mL^{-1})was added to each well and incubated for 4 h. 100 μL DMSO was added into each well after the solution contains MTT was discarded. Absorbance at 570 nm was measured by a microplate reader.

2.6. Lipid extraction and sample preparation

Lipid was extracted using Folch method [50] with minor modification. A mixed solution containing 150 μL DI water, 190 μL methanol, and 340 μL dichloromethane was used as the extractant. The frozen cell pellets containing 1×10^6 cells for each cell line were suspended into the extraction solution and vortexed for 5 min, and then centrifuged at ~2500 g for 5 min to isolate the bottom layer. 30 μL of the extracted lipids were dropped on the sample spots of the NALDI target. The lipid profile of each cell line was acquired on 5 replicated sample spots, and 2 spectra were collected on each spot. For the tissue sample, lipids were extracted from cut tumor tissues with a diameter of 2 mm using the same method as described above.

2.7. NALDI-MS analysis

NALDI-MS analysis was performed using an UltrafleXtreme MALDI-TOF/TOF instrument (Bruker Daltonics Corp) equipped with a 355 nm Nd: YAG laser beam (pulse width = 3 ns). The NALDI target was fixed onto a costume-made plate designed to match with the MALDI-TOF-MS instrument. Mass spectra were acquired under reflecting negative ion mode at the *m/z* range of 200–1000 Da. The laser pulse energy was set at 16 μJ, and it was 79% of the maximum energy. Other instrument parameters were set as follows: 120 ns pulsed ion extraction, 25 kV (ion source 1) and 23.65 kV (ion source 2) acceleration voltage. A mixture sample of C12:0, C16:0, C18:0, C20:0, C24:0 and DPPE was used for mass calibration at negative ion mode. 1500 laser shots were averaged for each mass spectrum.

2.8. LC-MS/MS identification

The extracted lipids of the five HCC cell lines were analyzed by AB Triple-TOF 5600plus System (AB SCIEX, Framingham, USA) coupled with Waters UPLC system. Dichloromethane in each sample was removed by nitrogen stream, and then the dried sample was diluted with 50 μL methanol and isopropyl alcohol (v/v = 1:1). 5 μL aliquot sample was injected into the UPLC system equipped with an Agilent SB-C18 column (3.5 μm, 2.1 × 100 mm, Agilent Corp.) at 40 °C. The mobile phase A was 50% acetonitrile aqueous solution dissolved with 5 mM ammonium formate and 0.1% formic acid and mobile phase B was 5% acetonitrile in isopropanol dissolved with 5 mM ammonium formate and 0.1% formic acid. Liner gradient flow condition is as follows: 0.5 min of 80% mobile phase A, 7 min of 20%–50% mobile phase B, 50% to 80% mobile phase B in 2.5 min, 80% to 100% mobile phase B in the next 10 min and maintain 100% mobile phase B for 1.9 min, 100% to 20% mobile phase B for 0.1 min, and 80% mobile phase A for 3 min. The flow rate of mobile phase was 400 μL min^{-1}. Mass spectra were acquired at the *m/z* range 100-1,500 with a resolving power setting of more than 40,000 [51].

2.9. Data analysis

The baseline of original mass spectrum data was smoothed and then exported to txt file from FlexAnalysis (Bruker Daltonics Corp). SPSS Ver. 22 (IBM, Chicago, IL, USA) was used for one-way analysis of variance. Several home-developed programs based on MATLAB were used for principal component analysis (PCA), hierarchical clustering analysis (HCA), linear discriminant analysis (LDA) and Pearson correlation coefficient analysis. For each ion peak, there are two judging criteria to input the peak data for subsequent multivariate statistical analysis: (1) signal-to-noise (S/N) ratio of the peak is greater than 5; (2) the frequency of occurrence in the spectrum of the same cell line is greater than 66%. LIPID MAPS® online tools [52] and the Human Metabolome Database (HMDB) [53] were used to find the information of parent ions with the corresponding MS/MS data.

3. Results and discussion

3.1. Preparation and characterization of NALDI target

A schematic procedure for the preparation of NALDI target and its application in cell lipid profiling was illustrated in Scheme 1. The pattern of NALDI target is shown in Fig. 1a and b. In the present work, metal-assisted chemical etching (MACE) was adopted to etch the Si NWs on each sample spot. The length and diameter of silicon nanowires can be adjusted by controlling the concentration of HF and silver ions in the etching solution and the length of etching time. After optimizing the etching condition, the NALDI target etched in 4.8 M HF and 0.02 M $AgNO_3$ aqueous solution for 10 min was chosen as the best condition, because the target displayed best performance for cell lipid detection (Fig. S1). The vertical silicon nanowires prepared under this etching condition have a length of about 1.5 μm and a diameter of about 50 nm, as shown in scanning electron microscopy (SEM) images (Fig. 1c and d).

To compare the MS detection performance, a standard sample containing mixture of standard lipids (C16:0, C18:0, C20:0, C24:0, each fatty acid has the same concentration at 100 μg mL^{-1}) was detected on NALDI target and non-array target, respectively. Both type of targets displayed great ability in lipid detection and negligible background interference (Fig. 1e). Without using organic matrix such as CHCA or DHB, the interference caused by matrix molecule ion peaks and uneven distribution of analytes caused by co-crystallization can be avoided (Fig. S2). However, compare to the non-array target, the NALDI target showed better repeatability in the detection of mixed fatty acids standard solution. The relative standard deviation (RSD) of normalized intensity on NALDI target was significantly lower than that on non-array target (Fig. 1f). The linearity of C12:0 was studied on the NALDI target. A good linear relationship was achieved in the concentration range of 0.3 μg mL^{-1} to 40 μg mL^{-1} with coefficient of 0.9962 (Fig. S3). The limit of detection (LOD) of C12:0 was calculated to be 4.0 ng mL^{-1} (S/N = 3), indicating the high sensitivity of lipid detection on the NALDI target.

3.2. Lipids profile and potential biomarkers in five types of HCC cell lines

Lipids extracted from the 5 types of HCC cell lines by liquid-liquid extraction (LLE) method were profiled by NALDI-MS to select potential biomarkers that can distinguish each cell line. Fatty acids, phosphatidylcholine (PE, PI, PG, PA, PS) and glycosphingolipid (LacCer, ST) can be detected in negative ion mode since these components contain negative charged moiety such as carboxyl groups, phosphate group or sulfonic acid group. Fig. 2a shows the representative NALDI-MS profile of the lipids extracted from the 5 types of HCC cell lines with the total cell number of 1×10^6. Each cell lipid profile contains more than 200 mass peaks with *S/N* larger than 5. For each cell line, lipids extracted from three independent cultured cell samples were detected and 30 mass spectra were collected with good repeatability and stability (Fig. S4). According to the different abundance and *m/z* of ion peaks in mass spectra, they were divided into 20 ion peak clusters with different *m/z* range. All the 150 mass spectra were analyzed and the relative intensity of each peak was normalized within its cluster. The adjacent peaks who sharing the similar structure and with

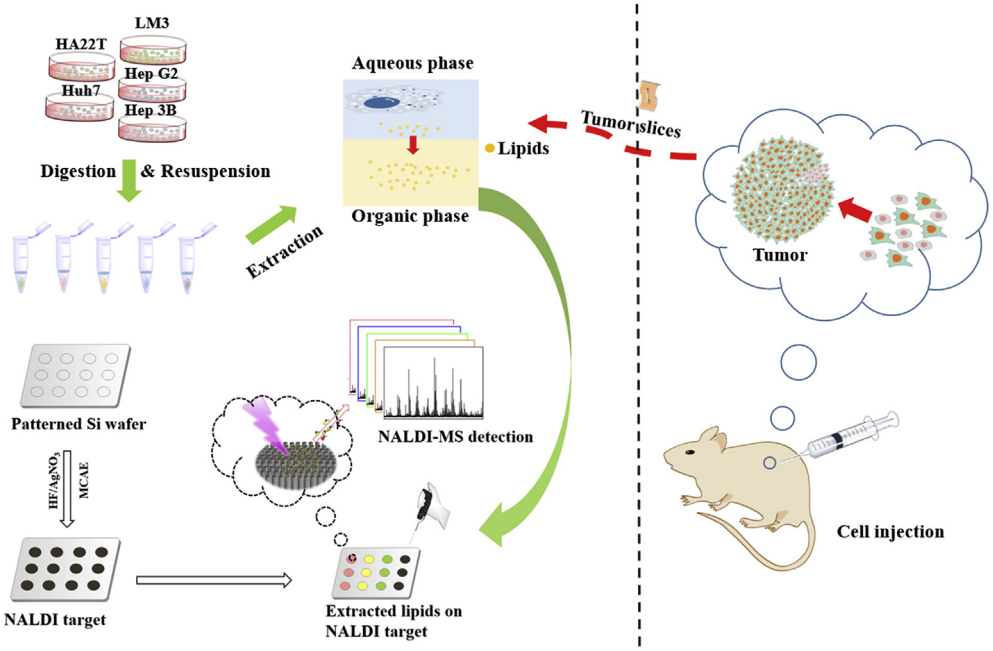

Scheme 1. Schematic procedure for the fabrication of NALDI target and the method for the NALDI-MS analysis of cell/tissue samples.

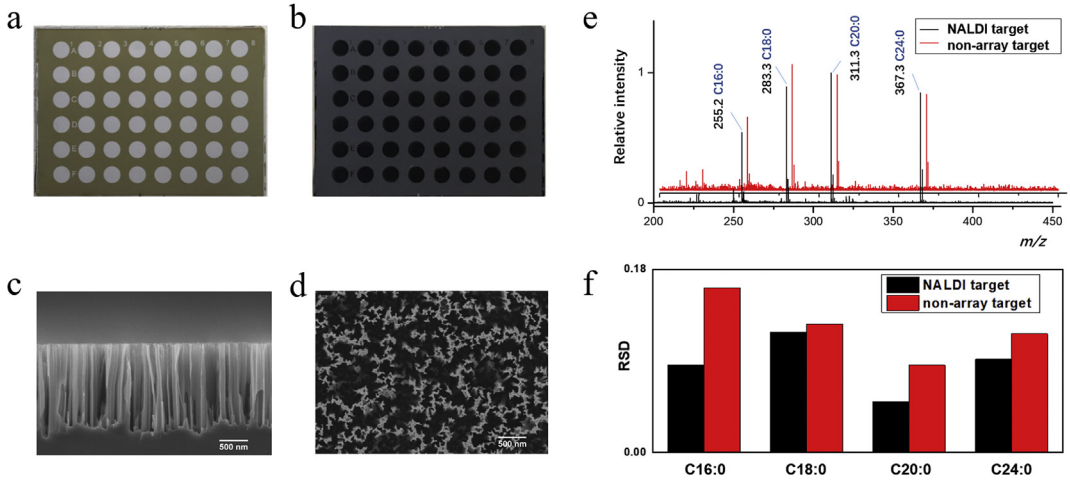

Fig. 1. (a) Spots array on AZ layer coated silicon wafer after photolithography. (b) The NALDI target contains 48 spots of silicon nanowires array prepared by the one-step metal-assisted chemical etching (MACE). (c) Cross-sectional scanning electron microscopy image of the vertical Si NWs. (d) Top view of the vertical Si NWs. (e) Mass spectra of C16:0, C18:0, C20:0, C24:0 detected on NALDI target and non-array target. (f) Relative standard deviation (RSD) of the signal intensities of C16:0, C18:0, C20:0, C24:0 detected on NALDI target and non-array target. 10 mass spectra were collected on NALDI target and non-array target, respectively. A mixed solution containing 100 μg mL^{-1} of each fatty acid was used in (e) and (f). (For interpretation of the references to colour in this figure legend, the reader is referred to the Web version of this article.)

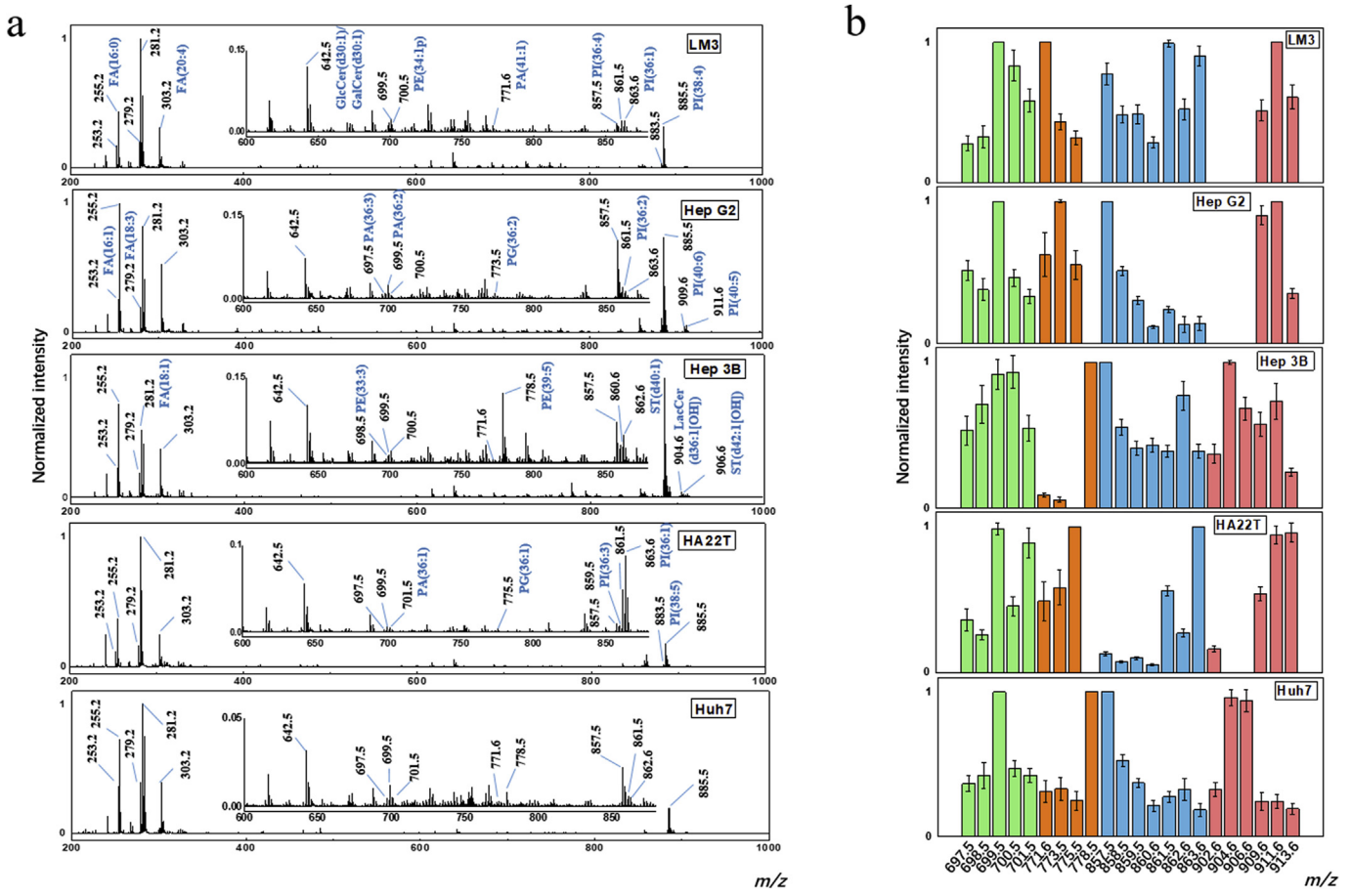

Fig. 2. (a) The representative NALDI-MS profile of the lipids extracted from the 5 HCC cell lines. (b) Relative intensity distribution of the 22 feature ions in each subtype of HCC cell line after normalization in their own clusters.

different degree of unsaturation were considered as the internal standards of each other. Compared with the normalization within full-spectrum (medium RSD: 30.76%), intensity normalization within each cluster can significantly enhance the stability and repeatability of the statistical analysis results obtained from different sample batch (medium RSD: 12.28%, Fig. S5). After the inner-cluster normalization, 22 ion peaks located in four clusters (*m/z* 697–702, *m/z* 701–779, *m/z* 857–864, *m/z* 902–914) were

sorted out by one-way analysis of variance in SPSS (IBM, Chicago, IL, USA) and ClinProTools software (Bruker Daltonics Corp). The *P*-value of all 22 selected ion peaks were less than 1×10^{-6} (Table S1). In addition, these 22 feature ion peaks were identified by LC-MS/MS and their molecular information is shown in Table S1. LIPID MAPS® online tools [52] was used to match the information of precursor ions with the corresponding MS/MS data. Mass tolerance of both precursor ions and product ions were set at 0.05 Da. Under negative ion mode, complete molecule information of the precursor ions can be obtained by matching their MS/MS fragments of characteristic head, fatty acid chains and some neutral losses (Fig. S6). The results indicated that these feature peaks belong to several types of phospholipids including PA, PE, PG, PI, PS and glycosphingolipids like LacCer, ST, which also appear in the MALDI-MS lipid profile of mammalian cells [23]. Some monoisotopic ion peaks were also identified and listed in Table S2.

In the peak cluster at the *m/z* range of 902–914, three unique lipid ions at *m/z* = 902.6 [LacCer(d37:1)-H]$^-$, 904.6 [LacCer(d36:1[OH])-H]$^-$ and 906.6 [ST(d42:1[OH])-H]$^-$ appeared in both Hep 3B cells and Huh7 cells with high intensity, while the ion peak at *m/z* = 902.6 [LacCer(d37:1)-H]$^-$ appeared in the HA22T cells with low relative intensity. Lipid profiles of LM3 cells, Hep G2 cells and Ha22T cells contained another three feature ions at *m/z* = 909.6 [PI(40:6)-H]$^-$, 911.6 [PI(40:5)-H]$^-$ and 913.6 [PI(40:4)-H]. Lipid ion at *m/z* = 778.5 [PE(39:5)-H]$^-$ in the peak cluster at the *m/z* range of 701–779 also appeared in both Hep 3B cells and Huh7 cells uniquely. Other 15 selected feature ions appeared in all lipid profiles of each cell line with different relative intensities (Fig. 2b).

The different distribution of lipids with different species will affect the fluidity and domain formation of cell membrane, thereby affecting migration, proliferation, and apoptosis of cells. Saturation status of lipids is closely related to packing and fluidity [54,55]. It should be noted that, among the four clusters, some of the lipid biomarkers in each cluster were the same type of lipid molecules with different unsaturation degree, their abundance may involve in the subtype-relating differences of HCC cells membrane.

3.3. Distinguishing the HCC cell subtypes

Principle component analysis (PCA) was analyzed by MATLAB using the panel of 22 feature ion peaks. The result showed that five types of HCC cell lines were classified into their respective regions with good concentration of data points within each cell line (Fig. 3a). Hierarchical clustering analysis (HCA) also showed that the five cell lines can be accurately discriminated from each other using these feature ion peaks with an accuracy rate of 100% (Fig. 3b). The statistical results prove the outstanding ability of these feature ion peaks to classify cell subtype, which is comparable to previous biotyper approaches [22–25] in the discrimination of cell subtypes. To compare the repeatability of PCA results obtained from inner-cluster normalization and full-spectrum normalization, the lipids profiles of LM3 cells and Huh7 cells were measured by 3 parallel MS detection. The PCA result using the inner-cluster normalized data of the 22 feature peaks displayed good repeatability (Fig. S7a). In contrast, PCA result exhibited poor repeatability among the parallel detection if using the full-spectrum normalized data (Fig. S7b), in which 11 feature ion peaks were sorted out by Student's t-test and ClinProTools (Table S3).

Combining the feature ion peaks selected by the two methods above, their relative intensities in the overall spectrum reflected significant difference among the five subtypes of HCC cell lines (Fig. S8). The diverse relative abundances of various lipids between cell lines may indicate the differences in energy storage, signal transduction, cell growth and proliferation of different subtypes indirectly.

3.4. Distinguishing the dominant HCC cell subtype in mixed cells

A clinical tumor tissue may contain multiple subtypes of cancer cells, so it is important to identify the dominant cancer cell subtype for precise medication guidance and prognosis. To test the effectiveness of cell subtype identification based on the 22 feature ion peaks, LM3 cells and Huh7 cells were mixed at the ratio of 1:0, 3:1(L3H1), 1:1(L1H1), 1:3(L1H3), 0:1 and tested according to the procedure mentioned above. Finally, 15 mass spectra were collected for each sample. The radar charts show the relative intensities of 22 feature peaks normalized within the 4 peak clusters. Mixed samples of LM3 cells and Huh7 cells exhibited common peak characteristics of both cell lines, but the peak patterns of mixed cells were more similar to the cell line with higher proportion (Fig. S9a). The result of HCA also indicated the good correlation between mixed cell samples and individual cell lines (Fig. S9b) that mixed cell samples showed high similarity to the cell line which had a higher proportion in the samples. Although the mixed cell sample of LM3:Huh7 = 1:1 had equal proportion for each cell line, its characteristic was more similar to Huh7 cell line than to LM3 cell, perhaps owing to the different lipid content of Huh7 cells and LM3 cells. If employing mathematical algorithm [56], different cell lines could also be discriminated according to the combined lipid spectrum of multiple cell lines. These results indicated that the established method has the potential to identify cell subtype with high proportion in mixed cell sample. Additionally, two ion peaks (*m/z*

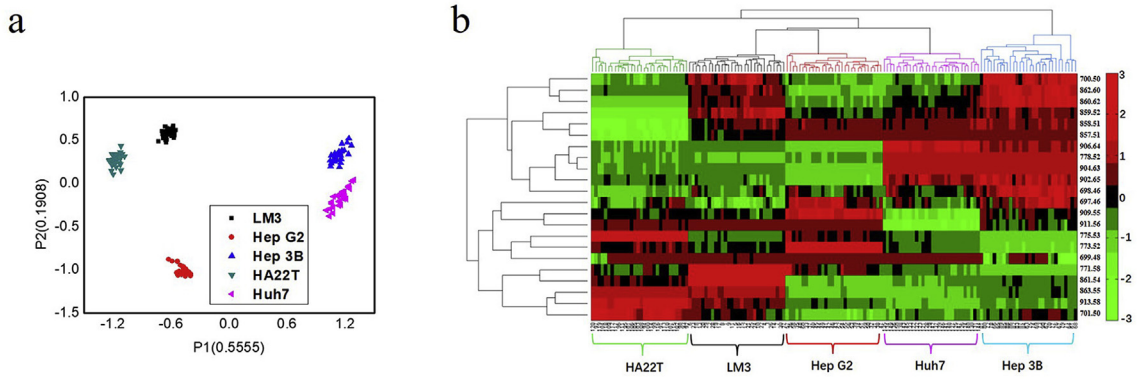

Fig. 3. Multivariate statistical analysis of the five HCC cell lines using the normalized intensities within clusters of the twenty-two feature ion peaks. (a) Principle component analysis (PCA) result. (b) Hierarchical clustering analysis (HCA) result.

857.5 [PI(36:4)-H]$^-$ and *m/z* 861.5 [PI(36:2)-H]$^-$) whose intensity ratio was linear related to the LM3 cell ratio were found ($R^2 = 0.9640$, Fig. S10). The ratio of the two peaks can potentially be used to determine the percentage of identified cell line in mixed cell samples [57].

3.5. Distinguishing the dominant HCC cell subtype in tissues

As we know, the growth environment of tumor tissue is more complex than cells cultured *in vitro*, so it is essential to verify the ability of these 22 characteristic peaks to judge the cell subtypes in tumor tissues. After a standard xenograft procedure with different cell injection ratio of LM3:Huh7 = 1:0, 3:1(L3H1), 1:3(L1H3), and 0:1, the four types of tumor tissues were collected from the male mice. Lipids were also extracted by the same method as that used in cell lipid extraction. The overall lipid profiles exhibited little difference compared to the profiles of cultured cells (Fig. S11). When we focused on the four cluster peaks where the 22feature ions located, their relative distribution within clusters was found to be very similar to their relative distribution in the lipid profiles of cultured LM3 or Huh7 cells (Fig. 4a).

Pearson's correlation coefficients between cell samples and tissue samples were calculated based on inner-cluster normalized data of the 22 feature ion peaks (Fig. 4b), where a positive value (in red colour) meant a positive relationship between samples in row and column. The result showed the tumor tissue growth from LM3 cells or Huh7 cells presented high correlation with the cultured LM3 cells or Huh7 cells, indicating that the established method possesses the ability to identify cell subtype in tumor tissue.

When tumors were grown from mixed cells, the situation becomes more complicated. The tumor grew from mixed cells with the ratio of LM3: Huh7 = 3:1 showed high correlation to the cultured LM3 cells. However, if the tumor has grown from mixed cell with ratio of LM3: Huh7 = 1:3, it also showed a higher correlation to LM3 cells rather than to Huh7 cells (Fig. 4a). This phenomenon can be explained by the competitive growth of LM3 cells and Huh7 cells in tumor tissue. When adequate nutrient was supplied in the culture medium, cancer cells compete vigorously for nutrients. LM3 cells have higher metastatic potential and proliferation rate than that of Huh7 cells, thus despoiled more nutrient and space during the growth of tumor. As a result, the tumor tissue was occupied by large number of LM3 cells instead of Huh7 cells finally. The different results obtained in mixed cells cultured *in vitro* and *in vivo* inferred that the growth rate of mixed cells *in vitro* and *in vivo* behaved differently. The results above show that the established cell subtype recognition model can be successfully applied to the subtype identification of tumor tissues, extending the application of the biotyper approach from *in vitro* cell to *in vivo* tissue cells.

3.6. Anticancer drug susceptibility test using NALDI-MS

It has been proved that metabolic expression level of HCC cells and other cancer cells can be influenced by drug treatment [58,59]. To assess whether the cell subtype identification method has capability to indicate the drug response of the cell line, LM3 cells were treated with three concentration of sorafenib (0 [control], 0.312 μM, 5 μM) for 24 h. Results of MTT assay showed that the change in cell viability was insignificant at the drug concentration of 0.312 μM, while it decreased to 43% at the drug concentration of 5 μM (Fig. S12a). In contrast, the cell response to drug treatment measured on NALDI-MS was more sensitive. The lipid expression level of cells changed remarkably after drug treatment at three concentration levels. For example, the relative intensities of FA (16:0), FA (18:0) and FA (20:4) became higher in the drug-treated groups compared with the control group. Meanwhile, the abundance of FA (16:1) and FA (18:1) decreased in 5 μM sorafenib treated group, whereas FA (16:1) showed higher abundance in 0.312 μM sorafenib treated group (Fig. S12b). The abundance of these *de novo* FA synthesis relating fatty acids may reflect metabolic variance of LM3 cells after drug treated [60,61].

The PCA using the full MS data showed that the three groups of LM3 cells treated with different concentration of sorafenib can be discriminated from the original LM3 cells, and their distribution on the PCA map was related to drug concentration they were treated (Fig. 5a). However, when linear discriminated analysis (LDA) based on the 22 characteristic peaks was conducted, LM3 cell line treated with different concentration of drug clustered together, while the five subtype cells could still be well discriminated (Fig. 5b). The results indicated that the 22 characteristic peaks were highly stable and only related to the cell subtype. Pearson's correlation coefficients also confirmed the high capability of cell subtype recognition model based on the 22 feature peaks even though the cells were treated with anticancer drug (Fig. S12c). Therefore, the results

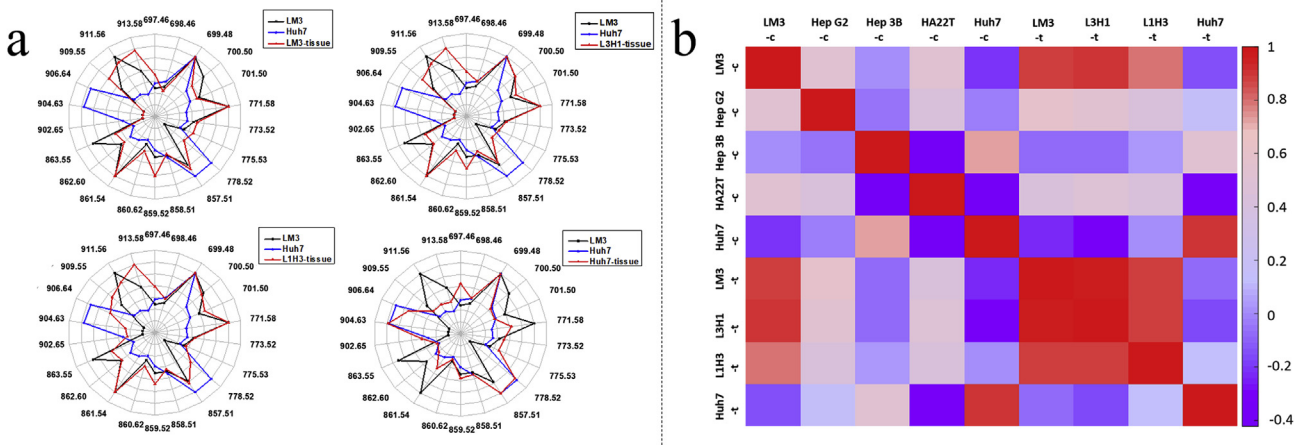

Fig. 4. (a) The radar charts comparing the relative distribution of the twenty-two ion peaks between different tumor tissues (LM3, L1H3, L3H1, Huh7) and cultured LM3/Huh7 cells. (b) Pearson's correlation coefficients between the five HCC cell lines and tumor tissues generated from different mixed ratio of LM3 and Huh7, using the relative intensity data within clusters of their twenty-two feature ion peaks. Cell samples have the suffix "–c" and tissue samples have the suffix "–t". Red represents positive correlation and purple represents negative correlation. (For interpretation of the references to colour in this figure legend, the reader is referred to the Web version of this article.)

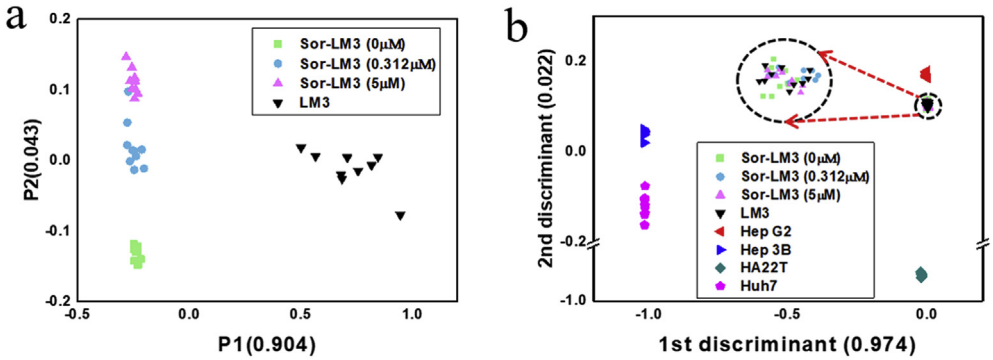

Fig. 5. Multivariate statistical analysis of previous LM3 cells and three groups of LM3 cells treated with drug. (a) Principal component analysis (PCA) result based on the normalization intensities of all ion peaks in entire spectrum; (b) Linear discriminated analysis (LDA) result based on the inner-cluster normalized intensities of 22 characteristic peaks. Data form 10 spectra were used for each group.

demonstrated that the NALDI platform can not only recognize the cell subtype but also reveal the drug response in a more sensitive way.

4. Conclusion

Overall, we demonstrated that NALDI-MS using NALDI target comprising vertical Si NWs is a high throughput and sensitive platform, which could profile lipids of 5 HCC cell lines and tissues after simple extraction. With the assistance of multiple statistical analysis, 22 potential biomarkers with the capability to discriminate cell subtypes were sorted out and identified. We also found the method of inner-cluster normalization was more stable and accurate than the method of normalization within full-spectrum. The cell subtype recognition model based on the 22 characteristic peaks could effectively discriminate the cell subtype of mixed cell samples and xenogeneic tumor tissue in mice with high accuracy, thereby extending the biotype approach from *in vitro* cell to tumor tissue. In addition, the full lipid profile of LM3 cells could sensitively respond to the treatment of anticancer drug, while the pattern of the 22 feature peaks related to the type cell lines retained. Therefore, the approach can also be potentially applied in the screening of anticancer drug and drug susceptibility test. Owing to the advantages of high-throughput, simple procedures and good stability, the method established in this work will become an efficient platform in tumor biopsy, precision medicine and prognosis.

Declaration of competing interest

The authors declare that they have no known competing financial interests or personal relationships that could have appeared to influence the work reported in this paper.

CRediT authorship contribution statement

Tao Wang: Conceptualization, Methodology, Investigation, Data curation, Software, Formal analysis, Writing - original draft. **Xiaoming Chen:** Software, Visualization, Validation. **Chunyan Luan:** Visualization, Writing - review & editing. **Jianmin Wu:** Conceptualization, Resources, Funding acquisition, Writing - review & editing, Supervision, Project administration.

Acknowledgements

This study is supported by grants from the National Natural Science Foundation of China [grants number 21874118, 21575127].

Appendix A. Supplementary data

Supplementary data to this article can be found online at https://doi.org/10.1016/j.aca.2020.02.019.

References

[1] A. Forner, M. Reig, J. Bruix, Hepatocellular carcinoma, Lancet 391 (2018) 1301–1314.
[2] F.S. Collins, H. Varmus, A new initiative on precision medicine, N. Engl. J. Med. 372 (2015) 793–795.
[3] D. Wu, D.C. Wang, Y. Cheng, M. Qian, et al., Roles of tumor heterogeneity in the development of drug resistance: a call for precision therapy, Semin. Canc. Biol. 42 (2017) 13–19.
[4] N.D. Marjanovic, R.A. Weinberg, C.L. Chaffer, Cell plasticity and heterogeneity in cancer, Clin. Chem. 59 (2013) 168–179.
[5] K. Eason, A. Sadanandam, Molecular or metabolic reprograming: what triggers tumor subtypes? Canc. Res. 76 (2016) 5195–5200.
[6] L. Weiss, Cancer cell heterogeneity, Canc. Metastasis Rev. 19 (2000) 345–350.
[7] J.A. McQuerry, J.T. Chang, D.D.L. Bowtell, A. Cohen, et al., Mechanisms and clinical implications of tumor heterogeneity and convergence on recurrent phenotypes, J. Mol. Med. (Berl.) 95 (2017) 1167–1178.
[8] D.K. Lee, S.W. Choi, M.S. Kim, J.H. Park, et al., Discovery of differentially expressed genes related to histological subtype of hepatocellular carcinoma, Biotechnol. Prog. 19 (2003) 1011–1015.
[9] J.S. Lee, S.S. Thorgeirsson, Functional and genomic implications of global gene expression profiles in cell lines from human hepatocellular cancer, Hepatology 35 (2002) 1134–1143.
[10] J. Calderaro, G. Couchy, S. Imbeaud, G. Amaddeo, et al., Histological subtypes of hepatocellular carcinoma are related to gene mutations and molecular tumour classification, J. Hepatol. 67 (2017) 727–738.
[11] T. Yamashita, M. Forgues, W. Wang, J.W. Kim, et al., EpCAM and alpha-fetoprotein expression defines novel prognostic subtypes of hepatocellular carcinoma, Canc. Res. 68 (2008) 1451–1461.
[12] Y.F. Shan, Y.L. Huang, Y.K. Xie, Y.H. Tan, et al., Angiogenesis and clinicopathologic characteristics in different hepatocellular carcinoma subtypes defined by EpCAM and alpha-fetoprotein expression status, Med. Oncol. 28 (2011) 1012–1016.
[13] X.M. Dai, S.L. Yang, X.M. Zheng, G.G. Chen, et al., CD133 expression and a-fetoprotein levels define novel prognostic subtypes of HBV-associated hepatocellular carcinoma: a long-term follow-up analysis, Oncol. Lett. 15 (2018) 2985–2991.
[14] J. Bestard-Escalas, A. Maimo-Barcelo, K. Perez-Romero, D.H. Lopez, et al., Ins and outs of interpreting lipidomic results, J. Mol. Biol. 431 (2019) 5039–5062.
[15] V. Vantaku, S.R. Donepudi, D.W.B. Piyarathna, C. Sekhar Amara, et al., Large-scale Profiling of Serum Metabolites in African American and European American Patients with Bladder Cancer Reveals Metabolic Pathways Associated with Patient Survival, Cancer, 2019, pp. 921–932.
[16] M. Ros-Mazurczyk, K. Jelonek, M. Marczyk, F. Binczyk, et al., Serum lipid profile discriminates patients with early lung cancer from healthy controls, Lung Canc. 112 (2017) 69–74.
[17] A. Thomas, N.H. Patterson, M.M. Marcinkiewicz, A. Lazaris, et al., Histology-driven data mining of lipid signatures from multiple imaging mass spectrometry analyses: application to human colorectal cancer liver metastasis biopsies, Anal. Chem. 85 (2013) 2860–2866.
[18] S. Krautbauer, E.M. Meier, L. Rein-Fischboeck, R. Pohl, et al., Ceramide and polyunsaturated phospholipids are strongly reduced in human hepatocellular carcinoma, Biochim. Biophys. Acta 1861 (2016) 1767–1774.
[19] M. Woolman, A. Tata, D. Dara, J. Meens, et al., Rapid determination of the

tumour stroma ratio in squamous cell carcinomas with desorption electrospray ionization mass spectrometry (DESI-MS): a proof-of-concept demonstration, Analyst 142 (2017) 3250–3260.
[20] Z. Wu, J.C. Shon, K.H. Liu, Mass spectrometry-based lipidomics and its application to biomedical research, J. Lifestyle Med. 4 (2014) 17–33.
[21] B. Munteanu, C. Hopf, Emergence of whole-cell MALDI-MS biotyping for high-throughput bioanalysis of mammalian cells? Bioanalysis 5 (2013) 885–893.
[22] V. Serafim, A. Shah, M. Puiu, N. Andreescu, et al., Classification of cancer cell lines using matrix-assisted laser desorption/ionization time-of-flight mass spectrometry and statistical analysis, Int. J. Mol. Med. 40 (2017) 1096–1104.
[23] M.W. He, S. Guo, J.L. Ren, Z.L. Li, In situ characterizing membrane lipid phenotype of human lung cancer cell lines using mass spectrometry profiling, J. Canc. 7 (2016) 810–816.
[24] J. Hanrieder, G. Wicher, J. Bergquist, M. Andersson, et al., MALDI mass spectrometry based molecular phenotyping of CNS glial cells for prediction in mammalian brain tissue, Anal. Bioanal. Chem. 401 (2011) 135–147.
[25] X. Zhang, M. Scalf, T.W. Berggren, M.S. Westphall, et al., Identification of mammalian cell lines using MALDI-TOF and LC-ESI-MS/MS mass spectrometry, J. Am. Soc. Mass Spectrom. 17 (2006) 490–499.
[26] H.S. Kang, S.C. Lee, Y.S. Park, Y.E. Jeon, et al., Protein and lipid MALDI profiles classify breast cancers according to the intrinsic subtype, BMC Canc. 11 (2011) 465.
[27] I. Panderi, E. Yakirevich, S. Papagerakis, L. Noble, et al., Differentiating tumor heterogeneity in formalin-fixed paraffin-embedded (FFPE) prostate adenocarcinoma tissues using principal component analysis of matrix-assisted laser desorption/ionization imaging mass spectral data, Rapid Commun. Mass Spectrom. 31 (2017) 160–170.
[28] K. Schwamborn, R.M. Caprioli, MALDI imaging mass spectrometry–painting molecular pictures, Mol. Oncol. 4 (2010) 529–538.
[29] D. Zhou, S. Guo, M. Zhang, Y. Liu, et al., Mass spectrometry imaging of small molecules in biological tissues using graphene oxide as a matrix, Anal. Chim. Acta 962 (2017) 52–59.
[30] G. Schlosser, G. Pocsfalvi, E. Huszar, A. Malorni, et al., MALDI-TOF mass spectrometry of a combinatorial peptide library: effect of matrix composition on signal suppression, J. Mass Spectrom. 40 (2005) 1590–1594.
[31] X.L. Dong, J.S. Cheng, J.H. Li, Y.S. Wang, Graphene as a novel matrix for the analysis of small molecules by MALDI-TOF MS, Anal. Chem. 82 (2010) 6208–6214.
[32] M. Rainer, M.N. Qureshi, G.K. Bonn, Matrix-free and material-enhanced laser desorption/ionization mass spectrometry for the analysis of low molecular weight compounds, Anal. Bioanal. Chem. 400 (2011) 2281–2288.
[33] Y.F. Huang, H.T. Chang, Analysis of adenosine triphosphate and glutathione through gold nanoparticles assisted laser desorption/ionization mass spectrometry, Anal. Chem. 79 (2007) 4852–4859.
[34] A. Schnapp, A.C. Niehoff, A. Koch, K. Dreisewerd, Laser desorption/ionization mass spectrometry of lipids using etched silver substrates, Methods 104 (2016) 194–203.
[35] M. Dufresne, J.F. Masson, P. Chaurand, Sodium-doped gold-assisted laser desorption ionization for enhanced imaging mass spectrometry of triacylglycerols from thin tissue sections, Anal. Chem. 88 (2016) 6018–6025.
[36] J. Wei, J.M. Buriak, G. Siuzdak, Desorption-ionization mass spectrometry on porous silicon, Nature 399 (1999) 243–246.
[37] A.R. Korte, S.A. Stopka, N. Morris, T. Razunguzwa, et al., Large-scale metabolite analysis of standards and human serum by laser desorption ionization mass spectrometry from silicon nanopost arrays, Anal. Chem. 88 (2016) 8989–8996.
[38] J. Gao, M. de Raad, B.P. Bowen, R.N. Zuckermann, et al., Application of black silicon for nanostructure-initiator mass spectrometry, Anal. Chem. 88 (2016) 1625–1630.
[39] M. Dupre, C. Enjalbal, S. Cantel, J. Martinez, et al., Investigation of silicon-based nanostructure morphology and chemical termination on laser desorption ionization mass spectrometry performance, Anal. Chem. 84 (2012) 10637–10644.
[40] T.R. Northen, O. Yanes, M.T. Northen, D. Marrinucci, et al., Clathrate nanostructures for mass spectrometry, Nature 449 (2007) 1033–1036.
[41] M.J. Kang, J.C. Pyun, J.C. Lee, Y.J. Choi, et al., Nanowire-assisted laser desorption and ionization mass spectrometry for quantitative analysis of small molecules, Rapid Commun. Mass Spectrom. 19 (2005) 3166–3170.
[42] J. Sunner, E. Dratz, Y.C. Chen, Graphite surface-assisted laser desorption/ionization time-of-flight mass spectrometry of peptides and proteins from liquid solutions, Anal. Chem. 67 (1995) 4335–4342.
[43] A. Muck, T. Stelzner, U. Hubner, S. Christiansen, et al., Lithographically patterned silicon nanowire arrays for matrix free LDI-TOF/MS analysis of lipids, Lab Chip 10 (2010) 320–325.
[44] S. Colantonio, J.T. Simpson, R.J. Fisher, A. Yavlovich, et al., Quantitative analysis of phospholipids using nanostructured laser desorption ionization targets, Lipids 46 (2011) 469–477.
[45] V. Vidova, P. Novak, M. Strohalm, J. Pol, et al., Laser desorption-ionization of lipid transfers: tissue mass spectrometry imaging without MALDI matrix, Anal. Chem. 82 (2010) 4994–4997.
[46] A. Tata, A.M.A.P. Fernandes, V.G. Santos, R.M. Alberici, et al., Nanoassisted laser desorption-ionization-MS imaging of tumors, Anal. Chem. 84 (2012) 6341–6345.
[47] G. Luo, Y. Chen, H. Daniels, R. Dubrow, et al., Internal energy transfer in laser desorption/ionization from silicon nanowires, J. Phys. Chem. B 110 (2006) 13381–13386.
[48] J.A. Stolee, B.N. Walker, V. Zorba, R.E. Russo, et al., Laser-nanostructure interactions for ion production, Phys. Chem. Chem. Phys. 14 (2012) 8453–8471.
[49] X. Chen, T. Wang, L. Lin, F. Wo, et al., Tip-Enhanced photoinduced electron transfer and ionization on vertical silicon nanowires, ACS Appl. Mater. Interfaces 10 (2018) 14389–14398.
[50] J. Folch, M. Lees, G.H. Sloane Stanley, A simple method for the isolation and purification of total lipides from animal tissues, J. Biol. Chem. 226 (1957) 497–509.
[51] H. Zhang, Y. Gao, J. Sun, S. Fan, et al., Optimization of lipid extraction and analytical protocols for UHPLC-ESI-HRMS-based lipidomic analysis of adherent mammalian cancer cells, Anal. Bioanal. Chem. 409 (2017) 5349–5358.
[52] E. Fahy, M. Sud, D. Cotter, S. Subramaniam, LIPID MAPS® online tools for lipid research, Nucleic Acids Res. 35 (2007) W606–W612.
[53] D.S. Wishart, D. Tzur, C. Knox, et al., HMDB: the human metabolome database, Nucleic Acids Res. 35 (2007) D521–D526 (Database issue).
[54] W.K. Subczynski, A. Wisniewska, Physical properties of lipid bilayer membranes: relevance to membrane biological functions, Acta Biochim. Pol. 47 (2000) 613–625.
[55] S. Zalba, T.L. Ten Hagen, Cell membrane modulation as adjuvant in cancer therapy, Canc. Treat Rev. 52 (2017) 48–57.
[56] D. Cheng, L. Qiao, P. Horvatovich, Toward spectral library-free matrix-assisted laser desorption/ionization time-of-flight mass spectrometry bacterial identification, J. Proteome Res. 17 (2018) 2124–2130.
[57] X.M. Chen, F.J. Wo, J. Chen, J. Tan, et al., Ratiometric mass spectrometry for cell identification and quantitation using intracellular "Dual-Biomarkers, Sci. Rep. 7 (2017).
[58] X. You, W. Jiang, W. Lu, H. Zhang, et al., Metabolic reprogramming and redox adaptation in sorafenib-resistant leukemia cells: detected by untargeted metabolomics and stable isotope tracing analysis, Canc. Commun. 39 (2019) 17.
[59] J.F. Zheng, J. Lu, X.Z. Wang, W.H. Guo, et al., Comparative metabolomic profiling of hepatocellular carcinoma cells treated with sorafenib monotherapy vs. Sorafenib-everolimus combination therapy, Med. Sci. Mon. Int. Med. J. Exp. Clin. Res. 21 (2015) 1781–1791.
[60] F.P. Kuhajda, K. Jenner, F.D. Wood, R.A. Hennigar, et al., Fatty acid synthesis: a potential selective target for antineoplastic therapy, Proc. Natl. Acad. Sci. U.S.A. 91 (1994) 6379–6383.
[61] B. Peck, Z.T. Schug, Q. Zhang, B. Dankworth, et al., Inhibition of fatty acid desaturation is detrimental to cancer cell survival in metabolically compromised environments, Canc. Metabol. 4 (2016) 6.